Journal of Alloys and Compounds 556 (2013) 188–197

Contents lists available at SciVerse ScienceDirect

Journal of Alloys and Compounds

journal homepage: www.elsevier.com/locate/jalcom

On the perfect MgH_2(–Nb,–Zr) systems and the influence of vacancy-like defects on their structural properties. A self-consistent first principle calculations study of the electron and positron parameters

C.R. Luna [a], E. Germán [a], C. Macchi [a], A. Juan [b,*], A. Somoza [c]

[a] IFIMAT, Universidad Nacional del Centro de la Provincia de Buenos Aires and CONICET, Pinto 399, B7000GHG Tandil, Argentina
[b] IFISUR, Dpto. Física, Universidad Nacional del Sur and CONICET, Av. Alem 1253, B8000 Bahía Blanca, Argentina
[c] IFIMAT, Universidad Nacional del Centro de la Provincia de Buenos Aires and CICPBA, Pinto 399, B7000GHG Tandil, Argentina

ARTICLE INFO

Article history:
Available online 29 December 2012

Keywords:
Magnesium hydride
DFT
Electronic structure
Positron annihilation
Vacancies

ABSTRACT

The electronic and structural properties of MgH_2 systems containing vacancies and Zr or Nb as dopants were studied using self-consistent calculations. The density of states were computed using the Vienna Ab initio Simulation Package (VASP) and the orbital overlap population weighted DOS with the Amsterdam Density Functional program. The metal–metal and metal–hydrogen bonds in the perfect hydride and this material containing a neutral Mg or H vacancies or a neutral mixed Mg–H vacancy complex were analyzed. The same calculations were also performed in the magnesium hydride with a Nb or a Zr atom as a substitutional impurity and on these systems containing the above mentioned vacancies. Simultaneously, the influence of vacancies in the hydride was studied through the calculation of the positron lifetimes and the positron–electron momentum distributions in the previously referred materials. Secondly, information on the influence of vacancies on the electron momentum density of the MgH_2(–Nb,–Zr) systems was additionally obtained through the calculation of the positron–electron momentum distributions. The results obtained indicate that in the pure hydride the presence of vacancies and impurities notable diminishes the force in the atomic bonds. The stability decrease of the bonds was correlated with changes in the positron wave function in the same sites of the structures. Moreover, it was found that these changes in the positron wave function are in good agreement with the decrease of the positron lifetimes.

1. Introduction

The use of fossil fuels has increasingly produced environmental pollution and carbon dioxide emissions. Great efforts are being made to develop sustainable and clean energy sources to replace the use of fossil fuels. One promising technology involves hydrogen stored in metal hydrides. Magnesium is one of the most promising materials for application in the hydrogen storage field and, therefore, has been the subject of extensive studies [1–3]. The use of hydrogen as an efficient, sustainable, and environmental friendly fuel requires wide spread innovation and development of the means for its production, storage and use [4]. The most promising hydrogen storage routes are solid-state materials that chemically bind or physically adsorb hydrogen at volume densities greater than those of liquid hydrogen. An ideal solid hydrogen storage material for a non-board storage system should meet the requirements of high performance (high H-capacity, fast kinetics and favorable thermodynamic properties), safety and cost effectiveness simultaneously [5–7].

As mentioned in our previous paper [8], magnesium hydride is a promising candidate for hydrogen storage. The doping of the MgH_2 with transition metals improves the kinetic of the hydrogen sorption process and accelerates the hydride- to- metal phase transition [9–12]. There are several experimental works considering Nb and Zr acting as dopant elements [9–14]. Song et al. analyzed the influence of the Nb on the MgH_2 stability. These authors attributed the loss of thermodynamical stability of the doped MgH_2 to a weakening of Mg–H bond [13].

It is well known that the diffusive processes in solids are assisted by vacancies. Recent theoretical works on Mg-based systems [15,16] and experimental studies on ball-milled Mg-based materials have suggested that the acceleration of the H_2 sorption kinetics could be also related to the presence of vacancy-like defects in these materials [17].

Positron Annihilation Spectroscopy (PAS) is a well-established high-sensitivity technique for detecting open volume defects in solids. It has been applied to the study of the defect structure for

* Corresponding author. Tel./fax: +54 291 4595142.
E-mail address: cajuan@uns.edu.ar (A. Juan).

0925-8388/$ - see front matter © 2012 Elsevier B.V. All rights reserved.
http://dx.doi.org/10.1016/j.jallcom.2012.12.121

almost 40 years, and is presently used in many fields of materials science. The physical principles of the study of lattice defects by PAS are discussed in [18]. Nevertheless, only few experimental or theoretical studies of defects in magnesium hydride or hydride-metal-phase transition were reported [8,19–21].

A preliminary theoretical study, using semiempirical and non self-consistent calculations, on the influence of vacancies of the electronic structure and bonding in pure MgH_2 doped with Nb was developed by the authors [8].

In this work, the topic previously treated is strictly analyzed in terms of a more precise calculation approach; i.e., self-consistent calculations were used. Specifically, the VASP (Vienna Ab Initio Simulation Package) code was used to compute the binding energy and the density of states while the crystal orbital overlap population was computed using ADF (Amsterdam Density Functional Program Package). Both the metal–metal and metal–hydrogen bonds in the perfect MgH_2 and in this material containing a Mg vacancy, a H one or a mixed Mg–H vacancy complex, were analyzed. The same calculations were also performed in the magnesium hydride containing a Nb or a Zr atom as substitutional impurities and on these systems containing the same kind of vacancies above mentioned. Simultaneously, the influence of vacancy-like defects in the different magnesium hydride systems was studied through the calculation of the positron lifetimes and the positron–electron momentum distributions.

2. Computational method

Electron and positron ab initio calculations have been performed within the frame of the density-functional theory (DFT) [22] which was implemented in the Vienna Ab initio Simulation Package (VASP) code [23,24]. The projector augmented wave (PAW) pseudopotential [23,24] was used to account the electron–ion core interaction, using the PW91 functional as the generalized gradient approximation (GGA) [25] for the exchange–correlation term.

The studied structures were simulated using a supercell containing 96 atoms (16 unit cells of MgH_2, see Fig. 1a). In the calculation, the Brillouin-zone was sampled using a $6 \times 6 \times 6$ Monkhorst-Pack $\boldsymbol{k}$-point mesh. [26]. For the plane-wave basis set a cut-off of 650 eV was used.

For the ionic relaxation, the forces acting on the ions were calculated using the Hellmann–Feynman theorem as the partial derivates of the free energy with respect to the atomic positions, including the Harris–Foulkes correction to the respective forces [27].

To obtain a full relaxation, all the structural degrees of freedom, including the volume and shape of the unit-cell and the atomic positions, were simultaneously relaxed. The relaxations were carried out using a conjugate gradient algorithm until the Hellman–Feynman force on each of the unconstrained atoms was less than 0.01 eV/Å. The self-consistent calculations were considered to converge when the difference in the total energy of the crystal between consecutive steps did not exceed 10^{-5} eV. In the same way, the static calculations were considered to converge using the same criterion.

To analyze the electronic structure and bonding we have used the concept of density of states (DOS) and the overlap population weighted DOS (OPDOS) [8,28–33].

2.1. Positron parameters

A general introduction to ab initio calculations of positron annihilation characteristics in solids can be found in Ref. [34]. However, to understand the meaning of some of the fundamental parameters representing positron annihilation in solids, a definition of the typical parameters representing the electro-positron annihilation process is given below.

The positron annihilation rate is defined as:

$$\lambda = \frac{1}{\tau} = \quad \pi r_e^2 c \int n_-(\vec{\mathbf{r}}) n_+(\vec{\mathbf{r}}) \gamma(n_-(\vec{\mathbf{r}})) d\vec{\mathbf{r}} \tag{1}$$

where r_e is the classical radius of electron, c the speed of light, $n_-(\vec{\mathbf{r}})$ the positron density, $n_+(\vec{\mathbf{r}})$ the electron density and $\gamma(n_-(\vec{\mathbf{r}}))$ the enhancement factor taking into account the pile-up of electron density at the positron. The inverse of the rate of positron–electron annihilation is the positron lifetime τ which can be directly obtained for the experiments. This is a very important advantage of PAS techniques; i.e., it is possible to directly compare experiments and theory. In each positron state i, the positron probes different electron densities leading to different positron annihilation rates λ_i. In a vacancy-like defect, the electron density is locally reduced and thus the trapped positron lifetime is increased compared to free positrons.

On the other hand, the momentum distribution of the annihilating positron–electron pairs $\rho(\vec{\mathbf{p}})$ can be calculated through the method based on a Jastrow-like approximation for the momentum distribution for each electron state i:

$$\rho(\vec{\mathbf{p}}) = \pi r_e^2 c \sum_i \gamma_i \left| \int e^{-i\vec{\mathbf{p}}\vec{\mathbf{r}}} \Psi_+(\vec{\mathbf{r}}) \Psi_i(\vec{\mathbf{r}}) d\vec{\mathbf{r}} \right|^2 \tag{2}$$

where γ_i is the constant electron-state-dependent enhancement factor, the so-called state-dependent scheme [34]. The enhancement factor is written as:

$$\gamma_i = \frac{\lambda_i^{LDA}}{\lambda_i^{IPM}} \tag{3}$$

where λ_i^{LDA} is the annihilation rate of the state i within the local density approximation (LDA) for the positron–electron correlation effect and λ_i^{IPM} is the annihilation rate within the independent-particle model (IPM). $\Psi_+(\vec{\mathbf{r}})$ and $\Psi_i(\vec{\mathbf{r}})$ are the wave functions of the positron and the electron of the orbital i, respectively. The momentum distribution $\rho(\vec{\mathbf{p}})$ due to the free-positron annihilations reflects the bulk electronic structure, while that due to trapped-positron annihilations reveals the open volume electronic structure (i.e., defect electronic structure). These distributions can be experimentally obtained using coincidence Doppler broadening technique (CDB) [35]. CDB produces very useful data regarding the spectrum of valence and

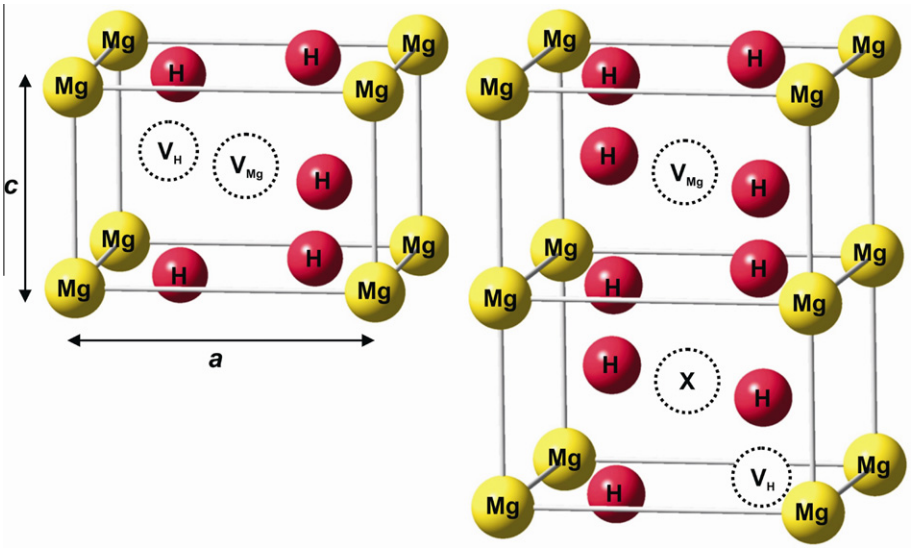

Fig. 1. (a) Hydride model supercell showing a H vacancy V_H, a Mg vacancy V_{Mg} and a Mg–H vacancy complex V_{Mg-H}. (b) X represents the location of the Nb or Zr substitutional impurity atom. (For interpretation of the references to colour in this figure legend, the reader is referred to the web version of this article.)

low-momentum core electrons. Distinctively, CDB can provide a chemically specific signal in the momentum distribution since core electrons retain their atomic character even in a solid.

In the present work, positron lifetimes and momentum distributions of the annihilating positron–electron pairs for positrons were calculated delocalized in the bulk or trapped in vacancy-like defects following the procedure developed by Makkonen et al. [36].

In all cases, to model the positron–electron correlation effects the LDA was used [37].

2.2. Hydride models

As a starting point of our models we have used the MgH_2 crystal structure determined by Park et al. [16] and Bortza et al. [38] and implemented by Luna et al. in Ref. [8]. The periodic magnesium hydride structures were generated from a 96-atoms supercell ($Mg_{32}H_{64}$). In this supercell different types of neutral vacancies were created (H vacancy, Mg vacancy, and the Mg–H vacancy complex), and two different types of substitutional impurities were incorporated, specifically either one Nb or one Zr atom (see Fig. 1b). A hydrogen or magnesium vacancy (named V_H and V_{Mg}, respectively) was created removing one H atom or one Mg atom. The Mg–H vacancy complex (V_{Mg-H}) was created removing from the structure one H atom and one Mg atom. The impurities were introduced in each structure by replacing one Mg atom by another Nb or Zr atom. In all cases, and in order to avoid edge effects, defects and impurities were located at the center of the supercell. Therefore, 12 structures were generated (see Table 1).

The supercell should be large enough in order to avoid the defect interaction with its periodic image; therefore, the system describes an isolated vacancy quite well. However, in practice, the size of the supercell cannot be built arbitrarily large. In order to calculate the positron characteristics, we have employed supercells considering periodic boundary conditions for the positron wave function. In all cases, the size of the supercell was gradually increased from 4 to 16 unit cells until convergences as in the positron lifetime (±0.1 ps) and as well as the energy per atom ($<10^{-5}$ eV) were obtained.

In this work, we have only considered neutral vacancies. However, it is well-known that charged vacancies can be present in a material producing a considerably change in its properties [39]. A vacancy of a given species can have different charge states, and this fact is relevant in terms of understanding the formation of antisite defects influencing, for example, the positron lifetimes in semiconductors [40,41]. A detailed study on the role of charged vacancies in the systems studied in the present work is a subject of an ongoing investigation.

3. Results and discussion

3.1. Geometric optimization

The calculated lattice parameters for the pure perfect MgH_2 cell: $a = 0.4501$ nm, $c/a = 0.6674$, and $u = 0.322$ nm were obtained from the ionic optimization. These results are in good agreement with the experimental values above mentioned.

On the other hand, the ionic relaxation around the different types of vacancies generated (V_H, V_{Mg} and V_{Mg-H} vacancy complex) for the pure and the doped systems was studied. To quantify the ionic relaxation, the relative changes in the volumes ΔV formed by the nearest-neighbor ions of a vacancy were estimated. Therefore, the ΔV values were obtained through $\Delta V = (V - V_0)/V_0$, where V is the volume in which the relaxed ion positions were taken into account and V_0 corresponds to the volume calculated when the ions are located in the ideal positions into each structure. In Table 2, the relative changes in the volumes are reported.

From the analysis of the results reported in Table 2, it can be concluded that when the pure hydride system contains a vacancy, independently of the type, a strong decrease in the ΔV is observed. This means that there is a shrinkage in the volume associated with the nearest-neighbor ions around a vacancy. On the other hand, for the doped-systems the relative changes in the volumes increase. This expansion is more important for the system containing Nb as substitutional atom. Moreover, when considering full relaxation it was found that the supercell sizes obtained did not substantially change (<1%); therefore, it could be concluded that vacancies did not influence the edges of the supercell. Hence, volume changes around vacancy-like defects and around impurity-like defects are significant; however, when defects are added at low concentration the total supercell size does not substantially change.

3.2. Density of states

In Fig. 2, the total and projected DOS curves obtained for the perfect MgH_2 structure (Fig. 2a) and this system containing Nb (Fig. 2b) or Zr as a substitutional atom (Fig. 2c) in its structure are shown. The transition metals mainly participate with their *d* electrons, *s* and *p* states have less contribution for the total densities of states of the hydrides. The most remarkable feature of the total DOS curves for these hydrides is that all exhibit semiconductor characteristics. The overall shapes of the total DOS are similar to each other; however, the position of the sharp peak or those peaks near the Fermi level is different. In MgH_2 the DOS curve shows a band gap of ~4 eV with a large dispersion of the bands signaling the *s*-like character. In the projected DOS curve for the H atom the intensity is due to the weight of H in the structure and also to the transfer of electrons from Mg to H leading to an ionic hydride. These DOS curves show a very good agreement with the results reported in Refs. [42,43].

When replacing a Mg atom by a Nb one in the MgH_2 structure, the DOS curve presents a narrow peak close to the Fermi level corresponding to the Nb *d* state (see Fig. 2b); while, when the Mg atom is replaced by a Zr one, in the corresponding DOS curve two peaks are observed: one close to E_F and another centered at a slight higher energy than the Fermi level, respectively, corresponding to the Zr *d* states (see Fig. 2c).

Xiao et al. [14] calculated DOS curves for $Mg_7H_{16}Nb$ and $Mg_7H_{16}Zr$ which show a similar trend to the results reported in the present work. However, there are some differences that can be attributed to the composition of the supercell chosen. Based on Xiao's work, it can be predicted that increasing the substituent concentration, the band gap width would decrease and the system would become conductor.

In Fig. 3, nine DOS curves for the MgH_2 systems (i.e., pure magnesium hydride and the structures doped with Nb or Zr) containing V_H, V_{Mg} or V_{Mg-H} are shown. When comparing the DOS curve for MgH_2–V_H (Fig. 3a) with that of the perfect hydride, the distinctive characteristic is the appearance of a sharp peak close to E_F, which corresponds to a contribution of the *s* and *p* states of Mg, and the *s* state of H. The top of valence band moves ~3 eV to lower energies below E_F. The substitution in the same system of a Mg atom by a Nb one, not only produces a broadening of the mentioned peak, product of the contribution of the *d* orbitals of Nb, but also a shift of the total DOS curve to higher energies (see Fig. 3b). A similar

Table 1
Atomic composition of the studied magnesium hydride systems.

Pure structures		Nb-structures		Zr-structures	
System	Composition	System	Composition	System	Composition
MgH_2	$Mg_{32}H_{64}$	MgH_2–Nb	$Mg_{31}Nb_1H_{64}$	MgH_2–Zr	$Mg_{31}Zr_1H_{64}$
MgH_2–V_{Mg}	$Mg_{31}H_{64}$	MgH_2–Nb–V_{Mg}	$Mg_{30}Nb_1H_{64}$	MgH_2–Zr–V_{Mg}	$Mg_{30}Zr_1H_{64}$
MgH_2–V_H	$Mg_{32}H_{63}$	MgH_2–Nb–V_H	$Mg_{31}Nb_1H_{63}$	MgH_2–Zr–V_H	$Mg_{31}Zr_1H_{63}$
MgH_2–V_{Mg-H}	$Mg_{31}H_{63}$	MgH_2–Nb–V_{Mg-H}	$Mg_{30}Nb_1H_{63}$	MgH_2–Zr–V_{Mg-H}	$Mg_{30}Zr_1H_{63}$

Table 2
Relative changes in the volumes formed by the nearest-neighbor ions of a vacancy for the systems: (a) MgH_2, (b) MgH_2–Nb and (c) MgH_2–Zr.

System	ΔV (%)	Doped system	Substitutional X = Nb ΔV (%)	Substitutional X = Zr ΔV (%)
MgH_2–V_H	−28	MgH_2–X–V_H	+6	+1
MgH_2–V_{Mg}	−26	MgH_2–X–V_{Mg}	+15	+6
MgH_2–V_{Mg-H}	−16	MgH_2–X–V_{Mg-H}	+9	+3

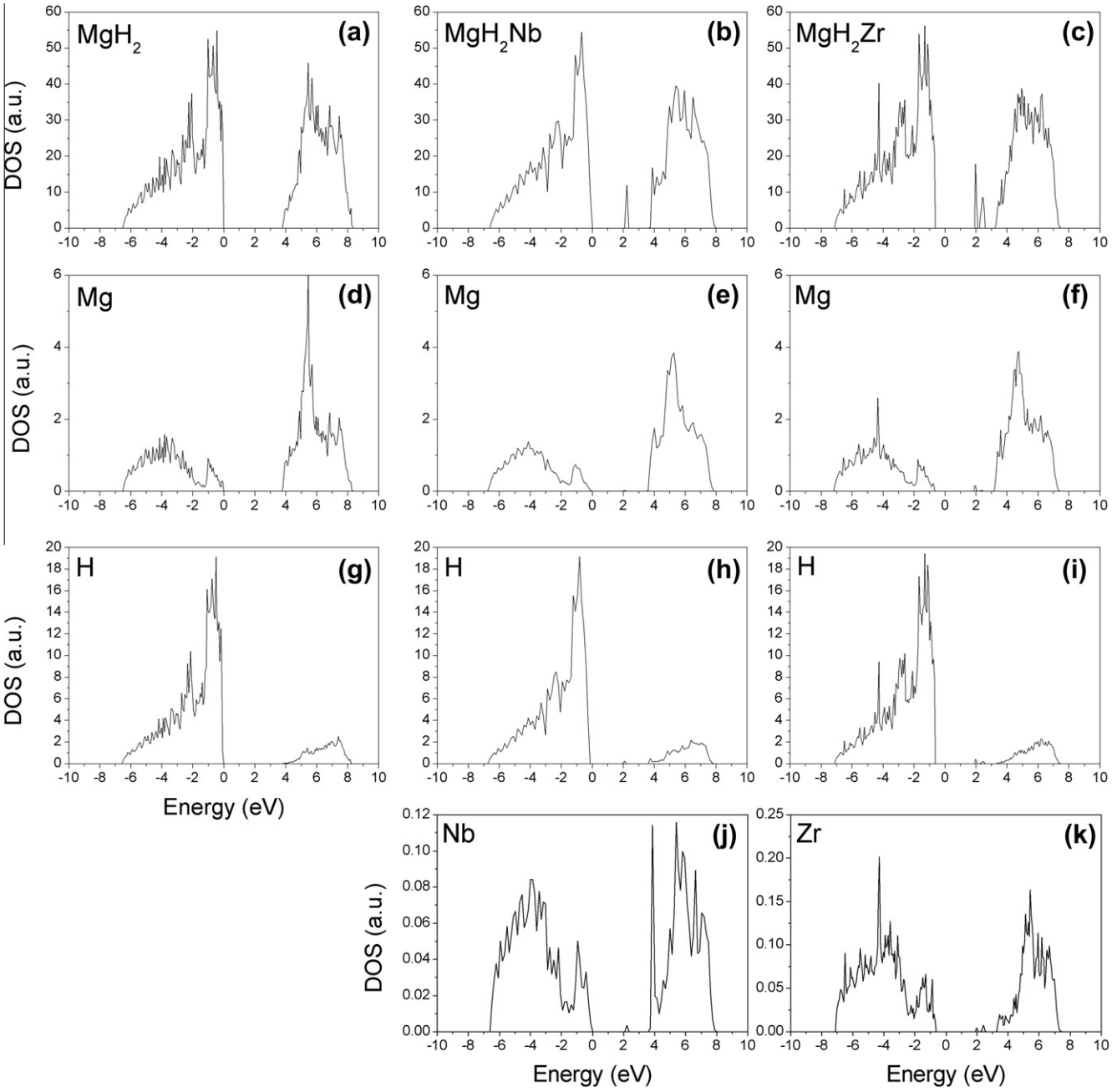

Fig. 2. Density of states curves calculated for MgH_2 (a), MgH_2–Nb (b) and MgH_2–Zr (c) systems and projected DOS curves corresponding to the different atoms.

trend in the DOS curve is observed when a Mg atom is substituted by a Zr one in the MgH_2–V_H. Besides, it seems that the previously mentioned peak would be split into two sharp peaks, corresponding to the Zr *d* states (see Fig. 3c). In the case of the DOS curve for MgH_2–V_{Mg} (Fig. 3d), from its comparison with that of the perfect hydride it can be concluded that, despite a similar trend in both curves two sharp and narrow peaks located at both edges of the band gap can respectively be seen. The peak located in the valence band corresponds to the H *s* state, and the peak in the conduction band corresponds to the Mg *s* state. The substitution in the MgH_2–V_{Mg} structure of a Mg atom by a Nb one (see Fig. 3e) generates at least three different sharp peaks located into the band gap, product

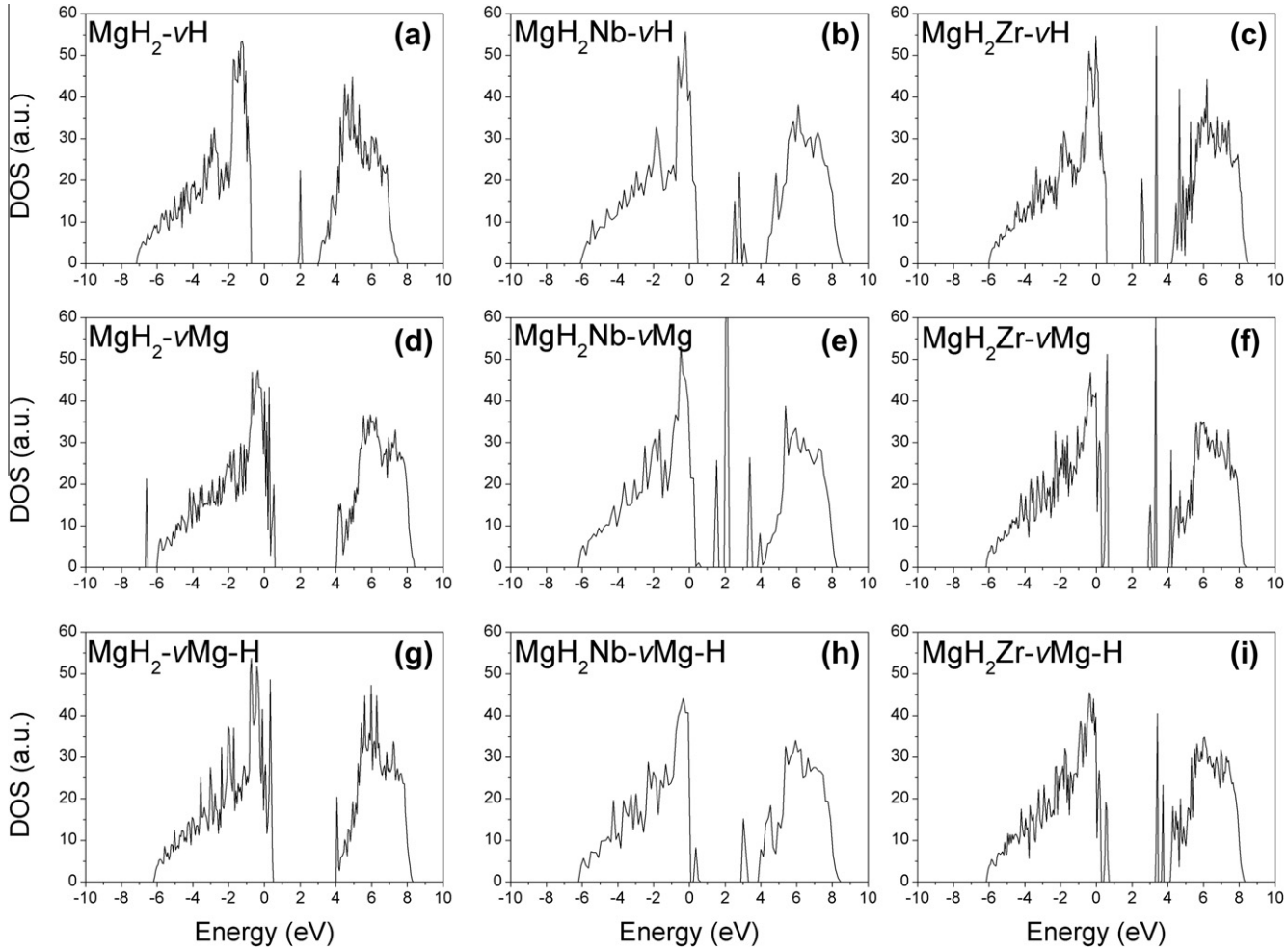

Fig. 3. DOS curves calculated for MgH_2–V_H (a), MgH_2–Nb–V_H (b), MgH_2–Zr–V_H (c), MgH_2–V_{Mg} (d), MgH_2–Nb–V_{Mg} (e), MgH_2–Zr–V_{Mg} (f), MgH_2–V_{Mg-H} (g), MgH_2–Nb–V_{Mg-H} (h) and MgH_2–Zr–V_{Mg-H} (i) systems.

of all states contribution but mainly to the Nb *d* state. In the case of a Zr atom replaces the Mg one (see Fig. 3f), the two sharp peaks observed at both edges of the band gap become stronger and the peak is located at the edge of the valence band corresponding to the contribution of the *s* orbital of H and the *s* and *p* orbitals of Mg. The peak located at the edge of the conduction band corresponds to the *d* orbitals of Zr; the same analysis can be made for the two near peaks located around 3 eV between the edges.

When comparing with the DOS curve calculated for the perfect MgH_2 presented in Fig. 2a, in the DOS curve for MgH_2–V_{Mg-H} (Fig. 3g) two sharp and intense peaks in the edges of the band gap appear, the peak at the edge of the valence band corresponds to the contribution of H and the peak at the edge of the conduction band corresponds to the contribution of the *s* state of Mg. It is important to point out that this effect is similar to that observed for the MgH_2–V_{Mg} structure. With the substitution of a Mg atom by a Nb one in the MgH_2–V_{Mg-H} structure (see Fig. 3h), into the band gap a broad peak at about 3 eV is observed and can be assigned to the contribution of the *d* state of Nb and the *s* state of Mg. Finally, when a Zr atom substitutes a Mg one (see Fig. 3i) a similar curve to that obtained for the MgH_2Zr–V_{Mg} system containing Zr is observed.

3.3. Overlap population

This analysis was carried out through the OP values for selected bonds, reported in Table 3. When a H vacancy is generated the Mg–Mg bonding strength significantly increases from 0.016 to 0.260, and the Mg–H bonds near *v*H become stronger in about 19.6% and 2.2% (from 0.230 to 0.275 and from 0.272 to 0.278), respectively. In the other hand, Mg–H bonds with a H atom far away from the vacancy weaken in about 5.2% and 13.6% (from 0.230 to 0.218 and from 0.272 to 0.235) , respectively.

In the case of a Mg vacancy, as well as Mg–H mixed vacancy complex case, Mg–Mg bonds weaken, the bond strength decreases about 62.5%, the Mg–H bonds with a H atom near to a V_{Mg} are strengthened in about 42.2% and 32.4%, respectively. The same behavior was observed for the Mg–H bonds with a H atom near to a V_{Mg-H} complex; i.e., 38.7% and 30.5%, respectively. The Mg–H bonds with a H atom far away from the vacancy are weakened. In the case of V_{Mg}, its strength decreases about 96.5% and 30.5%, respectively. For V_{Mg-H}, a decrease in the strength of the bond of 99.6% and 34.6% is observed.

When a Mg atom is replaced by a Nb one in the pure MgH_2, the formed Nb–H bonds are stronger than the Mg–H bonds, they increase 123.9% and 82.7%, respectively. Besides the Mg–H bonds decrease their strength about 10.9% and 46.3%, respectively.

Generating a V_H, the Mg–H bonds strength increases about 16.1% and 77.4%, Nb–H bonds with a H atom near to a *v*H are weakened approximately 11.1% and 24.1%, and the Nb–H bonds with a H atom far away from a V_H are strengthened 8.5%.

In the case of MgH_2–Nb–V_{Mg}, the Nb–Mg bonds are weakened as in the previous system, 0.093 versus 0.000 (see Table 3), the Mg–H bond strength increases about 36% and 83%. The Nb–H

Table 3
Overlap population for perfect MgH_2, Nb or Zr doped and vacancy containing hydride systems.

	MgH_2	MgH_2–V_H	MgH_2–V_{Mg}	MgH_2–V_{Mg-H}
Mg–Mg	0.016	0.260	0.006	0.006
Mg–H (4)	0.230	0.275[a]	0.327[a]	0.319[a]
		0.218[b]	0.008[b]	0.001[b]
Mg–H (2)	0.272	0.278[a]	0.360[a]	0.355[a]
		0.235[b]	0.189[b]	0.178[b]
	MgH_2–Nb	MgH_2–Nb–V_H	MgH_2–Nb–V_{Mg}	MgH_2–Nb–V_{Mg-H}
Mg–Nb	0.093	0.000	0.000	0.038
Mg–Mg	0.000	0.000	0.009	0.000
Mg–H	0.205	0.238	0.279	0.288[a]
				0.156[b]
Mg–H	0.146	0.259	0.266	0.266
Nb–H	0.515	0.559[a]	0.603	0.655[a]
		0.458[b]		0.442[b]
Nb–H	0.497	0.377	0.495	0.563
	MgH_2–Zr	MgH_2–Zr–V_H	MgH_2–Zr–V_{Mg}	MgH_2–Zr–V_{Mg-H}
Mg–Zr	0.027	0.000	0.000	0.022
Mg–Mg	0.005	0.000	0.010	0.025
Mg–H	0.225	0.272[a]	0.288	0.296[a]
		0.176[b]		0.187[b]
Mg–H	0.238	0.281[a]	0.267	0.358
		0.173[b]		
Zr–H	0.261	0.232	0.375	0.369
Zr–H	0.299	0.291	0.311	0.310

[a] Major OP value for this bond type.
[b] Minor OP value for this bond type, (4) Mg bonding to 4 equivalent H atoms, (2) Mg bonding to 2 equivalent H atoms.

bonds with a H near to the vacancy are strengthened ~17.1% and the Nb–H bonds with a H far away from a vacancy are weakened only 0.4%.

In presence of a Mg–H vacancy complex, some Mg–H bonds increase their strength while others decrease (+40.5%, +82.2% and −23.9%). Thus, the Nb–H bonds near to a V_{Mg} are 27.2% and 13.3% stronger than these bonds in the MgH_2–Nb system, and the Nb–H bonds near to the V_H decrease their binding force in 14.2%. These results are in good agreement with the tendency showed in previous calculations [1,8].

When replacing a Mg atom by another of Zr, the Mg–H bonds weaken in about 2.2% and 12.5%, respectively. On the other hand, the Zr–H bonds are 13.5% and 9.9% stronger than the Mg–H bonds in the pure MgH_2 system.

In MgH_2–Zr–V_H, the Zr–H bonds decrease their binding strength about 11.1% and 2.7%, respectively. Besides, the Mg–H bonds are weakened or strengthened depending on their location.

When a V_{Mg} is generated, the Mg–H bonds strengthen 28% and 12.2%, as well as the Zr–H bonds about 43.7% and 4%, respectively.

Finally, in MgH_2–Zr–V_{Mg-H}, the Zr–H bonds increase their strength. The Mg–H bonds near to the V_{Mg} are also strengthened approximately 31.6% and 50.4% and the Mg–H bonds near to the V_H are weakened ~26.7%.

3.4. Positron lifetimes

In Table 4, the calculated positron lifetimes for the different systems studied are reported. It can be observed that the different lifetimes for perfect structures are practically identical. Besides, the positron lifetime value for the pure magnesium hydride, τ_{MgH2} = 214.8 ps, is slightly lower than that of the bulk magnesium, τ_{Mg} = 218 ps. Therefore, it can be concluded that the substitution of one Mg atom by another Nb or Zr atoms does not basically change the τ values in each system; although the lifetimes for the bulk Nb (τ_{Nb} = 134 ps) and bulk Zr (τ_{Zr} = 164 ps) are about 40% and 25% lower than that of bulk Mg, respectively.

Table 4
Calculated positron lifetimes and percentage change in the lifetimes, with respect to the corresponding perfect systems.

System	τ (ps)	(%)	System	X = Nb		X = Zr	
				τ (ps)	(%)	τ (ps)	(%)
MgH_2	214.8	–	MgH_2–X	214.3	–	214.3	–
MgH_2–V_H	221.6	3.1	MgH_2–X–V_H	217.3	1	215.8	0.7
MgH_2–V_{Mg}	245.4	14.2	MgH_2–X–V_{Mg}	243.6	11	235.3	9.8
MgH_2–V_{Mg-H}	260.8	21.4	MgH_2–X–V_{Mg-H}	248.8	16.1	238.0	11.1

In the case of those hydride systems containing vacancies, both lifetime values for pure and doped structures depend on the type of vacancy being considered for the calculations. For pure hydride with a *v*H, the lifetime only increases about 3%; however, if the same structure has a *v*Mg, the calculated value of τ raises more than 14%. When a V_{Mg-H} complex is created in the pure hydride structure, τ grows more than 20% with respect to the perfect MgH_2 system. From the results reported in Table 4, it can also be concluded that the calculated positron lifetimes on the systems MgH_2–Nb and MgH_2–Zr containing vacancies are consistently lower than those calculated for the corresponding pure systems. It is interesting to note that when a Zr substitutional atom is present in the hydride systems, the positron lifetimes are systematically below to those obtained for systems containing a Nb atom as dopant impurity.

A general analysis of the results presented above for the twelve systems studied, allows us to conclude that positrons are preferentially annihilated in systems containing magnesium vacancies, and the presence of H in the complex V_{Mg-H} depletes the local electron density at the defect site. A same trend is observed for the doped systems but the changes in the respective positron lifetimes are lower than the values obtained studying the pure systems; this behavior can be attributed to the influence of the dopant transition metal elements on the local electron density around the defect sites. Specifically, there is an increase of the local electron density with a consequent decrease of the positron lifetimes.

When comparing the positron lifetimes calculated in the present work with those previously reported using non self-consistent methods for the MgH_2 and MgH_2–Nb systems (see Ref. [8]) it outcomes that only in the case of the perfect systems there exists an appreciable difference. The values obtained using the non self-consistent method are systematically above of those calculated using the self-consistent methods. This difference can be attributed to the fact that in the calculations performed in the present work the ionic relaxation was taken into account.

Positron data can also be analyzed in terms of the positron wave functions density of the system under study. These densities can be compared to the electron densities as follows.

In Fig. 4a a 2-D contour plot of the calculated positron wave function corresponding to the perfect magnesium hydride is presented. On the other hand, in Fig. 4b a 2-D contour plot of the electronic density for the same system is also shown. As can be seen, in the perfect lattice the positron wave function has its maxima at the interstitial regions and the wave function progressively vanishes toward the Mg and H ion-core regions. As a consequence, the Mg ion cores are more positive charged than the H ones, the progressive vanishing behavior is stronger for the Mg ion cores (see Fig. 4a). When comparing Fig. 4a with Fig. 4b, it can be seen that the region in which the electron density appears more depleted is in correspondence with the maxima for the positron wave function; i.e., positron probes a local electron density lower than the average electron density of the system.

In Fig. 5a and b the positron wave function and the electron density for the Nb-doped MgH_2 are presented, respectively. As

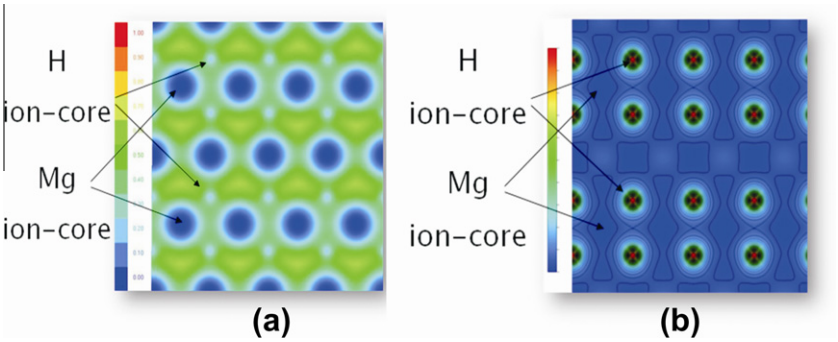

Fig. 4. 2D contour plot in perfect MgH_2 of the: (a) positron wave function and (b) electron density (the plots are presented in colors). The plane of the figures is the (−1 1 0) cut of the supercell used for the calculations. (For interpretation of the references to color in this figure legend, the reader is referred to the web version of this article.)

mentioned above, the positron lifetime calculated for this system is almost the same as that of pure MgH_2. However, as can be seen in Fig. 5a the presence of only one Nb atom in the magnesium hydride lattice is enough to modify the positron density around this atom. Specifically, in the darker regions around the Nb atom positrons probe a local electronic density higher than the average of the lattice (see Fig. 5b); this result would indicate a lower positron confinement than that corresponding to the undoped MgH_2. Besides, the change observed in the positron wave function is in good agreement with the decrease of the corresponding positron lifetime. The same tendency was observed when considering a Zr atom as dopant in the pure magnesium hydride system; therefore, the figures of the positron and electron densities are not shown here.

In Fig. 6a and b the same plots of Fig. 5 but for hydride system containing a Mg vacancy are presented. As can be seen in Fig. 6a, the positron wave function is clearly centered at the vacant site of the lattice and its level is almost two orders of magnitude higher than that of the perfect system. This result indicates a very strong positron confinement at the vacancy site. In such a case, it should be expected a strong increase of the positron lifetime with respect to that of the perfect MgH_2; in fact, from our calculations this parameter increases ∼11.5%. In Fig. 6b the electron density for the same system is shown. In this case, it can be seen a region labeled V_{Mg} in which the local electron density is depleted as a consequence of the vacant site. It is interesting to compare the figures representing the positron and electron densities calculated for the hydride magnesium containing one vacancy of Mg. Both plots are almost totally complementary indicating that both particles (positrons and electrons) are "seeing" the same effect.

In the case of the MgH_2–Nb system with a Mg vacancy, the respective positron and electron densities are qualitatively similar to those presented in Fig. 6 for MgH_2–V_{Mg}; therefore, the 2-D contour plots are not presented here. However, it is important to point out that the presence of a Nb atom around the Mg vacancy modifies the positron wave function; i.e., the electron density in this region becomes locally increased. In agreement with this result, the corresponding positron lifetime decreases (see Table 4).

3.5. Positron–electron momentum distributions

Since the positron–electron momentum curves span several orders of magnitude, it is usual to present the results in terms of a relative difference to a reference curve. In this paper, we choose the perfect pure magnesium hydride as the reference distribution. Such relative difference curves (RD curves) can contain one or more signature peaks, whose position, shape and height can be used to identify the chemical species (usually named "fingerprint" [44]) contributing to the RD curve.

Since there are not reported experimental studies with CDB technique on the present systems, the present interpretation of the calculated positron–electron momentum distributions must be taken as a first approach to the discussion on the role of the vacancies and the dopant on the structural properties of the MgH_2.

In Fig. 7a, the positron–electron momentum relative distributions for the magnesium hydride systems containing a dopant atom (Nb or Zr) substituting a Mg one are shown.

As can be seen, both distributions are very similar, this result seems to be very reasonable due to the fact that as Nb as Zr are transition metals and they are adjacent in the periodic table, consequently having a similar core structure. However, when comparing these RD curves with experimental and calculated distributions for pure metals and alloys (see for example Refs. [45–47]), it can be concluded that the RD curves for MgH_2–Nb and MgH_2–Zr give very

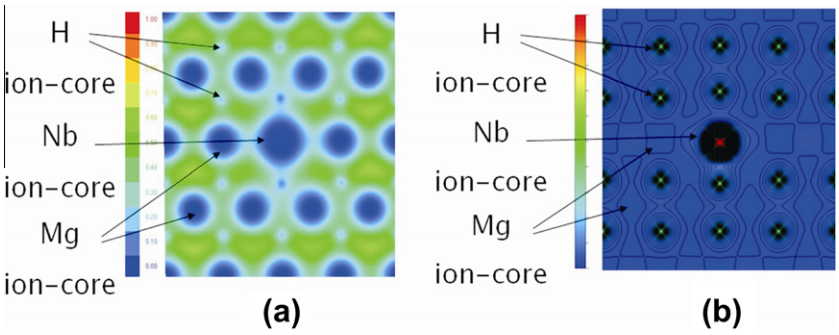

Fig. 5. 2D contour plot in a magnesium hydride containing a Nb atom (MgH_2–Nb) of the: (a) positron wave function and (b) electron density (the plots are presented in colors). The plane of the figures is the (−1 1 0) cut of the supercell used for the calculations. (For interpretation of the references to color in this figure legend, the reader is referred to the web version of this article.)

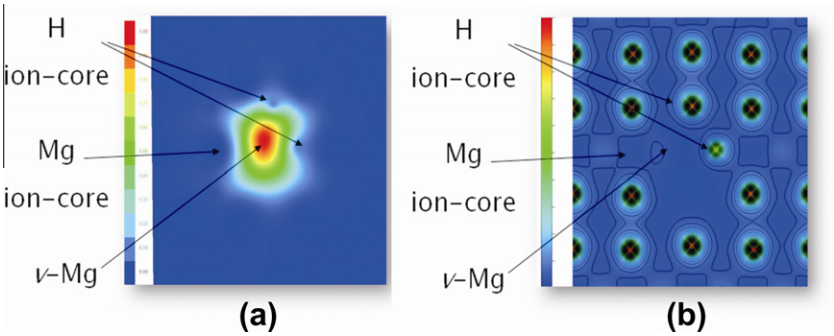

Fig. 6. 2D contour plot in magnesium hydride with a Mg vacancy (MgH_2–V_{Mg}) of the: (a) positron wave function; and (b) electron density (the plots are presented in colors in the online version). The plane of the figures is the (−1 1 0) cut of the supercell used for the calculations. (For interpretation of the references to color in this figure legend, the reader is referred to the web version of this article.)

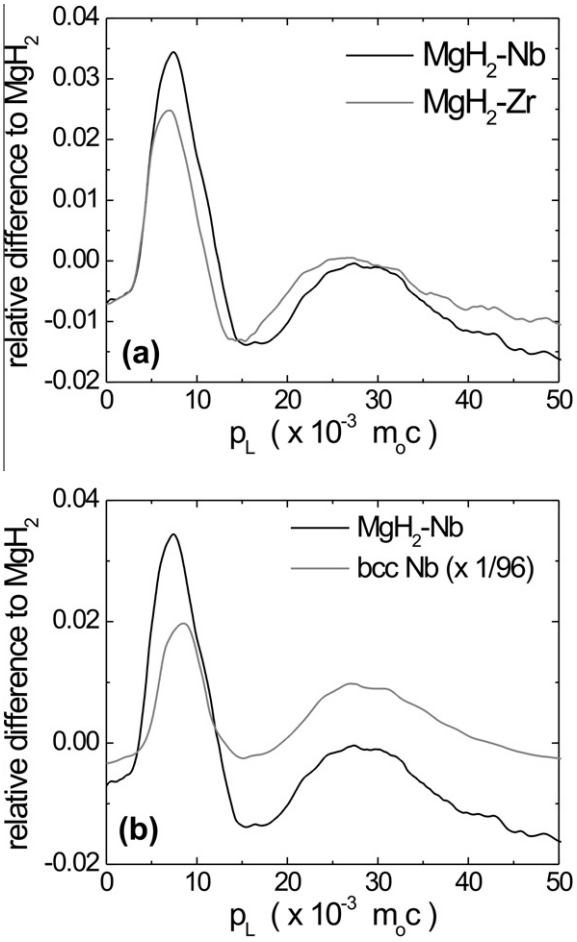

Fig. 7. (a) Relative difference of the momentum distribution of the annihilating positron–electron pair (RD curves) for the magnesium hydride doped with a Nb or Zr atom. (b) RD curves for pure bcc Nb and for Nb-doped magnesium hydride.

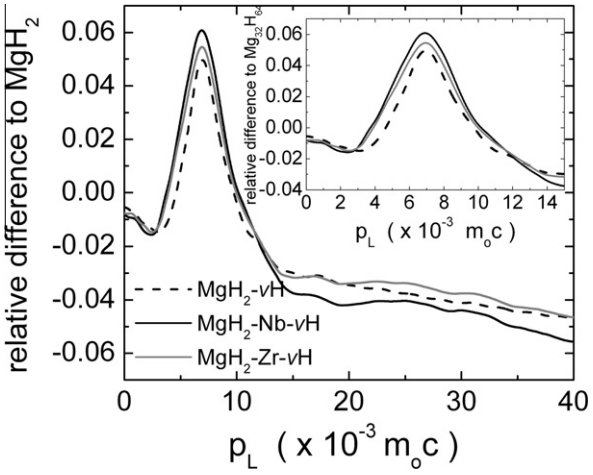

Fig. 8. Relative positron–electron momentum distributions of: (a) MgH_2–V_H, see dashed line, (b) MgH_2–Nb–V_H, see black solid line and (c) MgH_2–Zr–V_H, see gray solid line. Inset: the RD curves in the low momentum region are highlighted.

weak signals. As can be seen in Fig. 7b, the RD curve calculated for the magnesium hydride doped with a Nb atom is strongly dominated by the Nb fingerprint. The overall shape and the position of the peaks and valleys of the respective momentum distribution are practically identical despite we are dealing with different crystal structures. The small differences between both RD curves can be assigned to the different lattice structures (i.e., MgH_2–Nb is tetragonal while Nb is bcc). As a result, it could be concluded that the presence of Nb or Zr impurities in a very low concentration (at about 0.01 at.%) in the MgH_2 does not produce a significant change in the electron momentum density when compared to that of the pure hydride. These results show an excellent agreement with those obtained for the positron lifetime values (see Table 4).

In Fig. 8, the relative positron–electron momentum distributions of the magnesium hydride systems containing a H vacancy (V_H) are shown. In the inset, a detail of the RD curves in the low momentum region is also shown.

Accordingly to the usual analysis of CDB curves, the distribution corresponding to the pure MgH_2–V_H system near to $p_x = 0$ comes from the positrons annihilating with valence electrons. To higher momentum values, a peak located around $p_x = 7 \times 10^{-3}$ m_oc is observed. It can be attributed to the quantum confinement of the positron wave function in a region of atomic dimensions; specifically, a vacancy site (see Cizek et al. [47] and Calloni et al. [48]). For the high momentum region ($p_x \geqslant 20 \times 10^{-3}$ m_oc), the RD curve corresponds to positron annihilation with core electrons. In this region, the core contribution calculated was about 0.4% lower than that obtained for the perfect hydride (i.e., 8.1 % versus 8.5%).

The substitution of one Mg atom by another of Nb or Zr to the defected system containing a H vacancy does not noteworthy change the electron momentum distribution. These results are in good agreement with those obtained for the positron lifetime in the same systems.

In Fig. 9, the relative momentum distributions of the annihilating positron–electron pairs of the magnesium hydride systems containing a Mg vacancy are presented. In the inset, a detail of the RD curves in the low momentum region is also shown. From

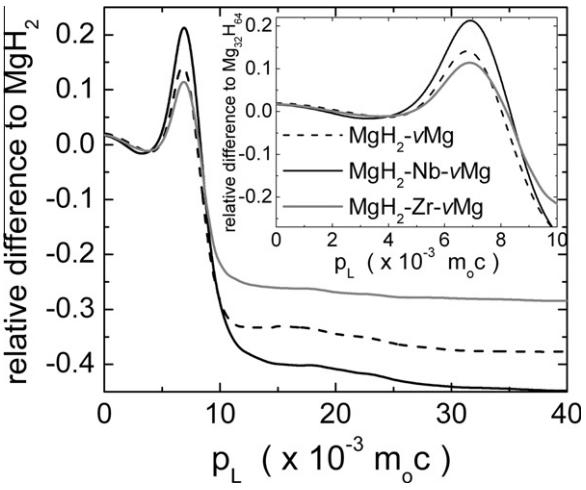

Fig. 9. Relative positron–electron momentum distributions of: (a) MgH_2–V_{Mg}, see dashed line, (b) MgH_2–Nb–V_{Mg}, see black solid line and (c) MgH_2–Zr–V_{Mg}, see gray solid line. Inset: the RD curves in the low momentum region are highlighted.

the comparison of this distribution with that of the MgH_2–V_H system reported in Fig. 8 (see dashed black line), it results that the presence of a Mg vacancy strongly changes the relative momentum distribution giving a higher signal. Furthermore, it can be observed that the corresponding localization peak is narrower than that obtained for MgH_2–V_H. Its maximum, centered at the same p_x value, is approximately 1.5 times higher than that of the MgH_2–V_H. The above described difference can be assigned to a higher confinement of the positron wave function. Regarding the high-momentum region, the RD signal of this system is about one order of magnitude stronger than that calculated for MgH_2–V_H. Specifically, it was found that the core contribution value obtained is almost half of that found for the magnesium hydride containing a H vacancy (i.e., 4.2% against 8.1%). Moreover, with the addition of the impurity substituent atoms the respective momentum distributions qualitatively do not show important differences. From the analysis of the relative curves, it can be concluded that when a Mg atom is removed from the pure magnesium hydride structure, an important change in the electron density at the vacancy site would be produced. It was also found that the simultaneously presence of a substitutional impurity with a Mg vacancy as nearest-neighbor, produces noteworthy changes in the respective electron momentum density at the vacancy site. This behavior is also observed in the positron lifetime calculated for the respective systems.

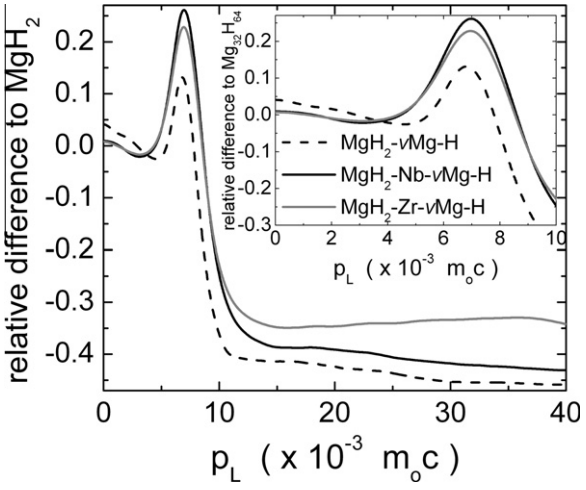

Fig. 10. Relative positron–electron momentum distributions of: (a) MgH_2–V_{Mg-H}, see dashed line, (b) MgH_2–Nb–V_{Mg-H}, see black solid line and (c) MgH_2–Zr–V_{Mg-H}, see gray solid line. Inset: the RD curves in the low momentum region are highlighted.

As can be seen in Fig. 10, the trends of the three RD curves corresponding to the magnesium hydride systems containing a Mg–H vacancy complex (V_{Mg-H}) are very similar to those described in Fig. 9. As a conclusion of these results, and in total agreement with the positron lifetime results, it can be said that the role of the Mg vacancy is dominant in the process of positron annihilation in a V_{Mg-H} complex.

4. Conclusions

In the present work, electronic and structural properties of magnesium hydride systems containing neutral vacancies and two different transition metals as dopants, specifically Nb and Zr atoms, were studied. To this aim, self-consistent first principle calculations were used to compute the crystal orbital overlap population for both the metal–metal and metal–hydrogen bonds in the perfect MgH_2 and in this system containing a Mg vacancy, a H one or a Mg–H vacancy complex. The same calculations were also performed in the above mentioned systems with a Nb or Zr atom as substitutional impurity and on these systems containing the same type of defects. In the twelve systems studied, VASP code was used to compute the electron density and the density of states; the crystal orbital overlap population was computed using the ADF package. In parallel, the influence of vacancies in the magnesium hydride systems were studied through the calculation of the positron lifetimes and the momentum distributions of the annihilating positron–electron pairs.

The main results can be summarized as follows:

- Regarding the density of states, it was found that:
  (a) In the perfect pure MgH_2 it was found that this material exhibits semiconductor characteristics. When this system is doped with Nb or Zr, the DOS curves present one or two peaks, respectively, into the band gap. The presence of these peaks was attributed to the *d* electrons of the transition metals. Besides, it was found that there is a systematic energy shift in the DOS curves toward lower energies in the doped hydrides; in such a case, it is reasonable to expect that the Mg–H bonds be easier to break in the doped systems.
  (b) In the systems containing vacancies, the DOS curves are strongly dependent on the type of vacancy created. In general, it was found that sharp and narrow peaks located at both edges of the band gaps appear. From these results, it was concluded that the peak located in the valence band corresponds to the H *s* state, while the peak located at the conduction band corresponds to the Mg *s* state. In the defected systems, peaks located into the band gap were also observed. This signal mainly comes from the *d* orbitals of the transition metal dopant.
- Regarding the overlap population, it was found that:
  (a) When the pure MgH_2 contains an impurity, the Mg–H bonds decrease their strength. This effect is stronger in the system containing Nb.
  (b) The presence of a vacancy in the three perfect systems strengthened the Mg–H bonds near the defect.
- Regarding the positron results, it was found that:
  (a) The positron lifetimes calculated for the pure magnesium hydride do not appreciably change with the addition of the impurities. However, the presence of a dopant atom in the structures, modifies the positron density around the impurity atom.

(b) For the systems containing vacancies, the positron lifetimes increase but they are strongly dependent on the type of vacancy. It is interesting to point out that the H vacancy does not significantly modify the local electron density at the defect site unless it is associated with a Mg vacancy. In particular, for the defected MgH_2–Nb and MgH_2–Zr the lifetimes are systematically below those calculated for the analogous pure systems; this behavior indicates that these impurities produce an increase in the local electron density in the defect.

- As a consequence that there are not reported experimental data from coincidence Doppler broadening on studies on magnesium hydrides systems, the calculated positron–electron momentum distributions in the present work must be considered as a first approach to a discussion on the role of vacancies and impurities on the structural properties of the mentioned systems.

(c) From the results obtained in the present work, it can be concluded that the presence of Nb or Zr impurities in a very low concentration (at about 0.01 at.%) in the perfect MgH_2 does not produce a significant change in the electron momentum density when compared to that of the pure hydride.

(d) In the magnesium hydride containing a Mg vacancy, it was observed an important change in the electron density at the vacancy site. Furthermore, it was found that the simultaneously presence of a substitutional impurity with a Mg vacancy as nearest-neighbor produces important changes in the respective electron momentum density at the vacancy site.

For each system studied, the results obtained from the analysis of the electron momentum distributions are in very good agreement with those of the calculated positron lifetimes.

A final and important remark regarding the main conclusions of the present work can be drawn from a comparative analysis of the 2D contour plots representing the positron wave function, obtained from positron calculations, and the electron density, obtained from electronic calculation. In fact, the results obtained for each system show that in every case both plots are absolutely complementary indicating that positrons and electrons revealed the same effect.

Acknowledgments

This work was partially supported by Agencia Nacional de Promoción Científica y Tecnológíca (Argentina) (PICT 2011-1088 and 2010-1770), Consejo Nacional de Investigaciones Científicas y Técnicas (Argentina) (PIP # 114-200801-00444), Comisión de Investigaciones Científicas de la Provincia de Buenos Aires, SECAT (UNCentro) and PGI- UNS SGCyT. AS and CM recognize the invaluable help of Dr. Ilja Makkonen in the use of MIKA and EPOS codes. We also want to express thanks to Teresita Maldonado for her technical help.

References

[1] L. Schlapbach, A. Züttel, Nature 414 (2001) 353–358.
[2] R.D. Cortright, R.R. Davda, J.A. Dumesic, Nature 418 (2001) 964–967.
[3] N.L. Rosi, J. Eckert, M. Eddaoudi, D.T. Vodak, J. Kim, M. O'Keeffe, O.M. Yaghi, Science 300 (2003) 1127–1129.
[4] G.W. Crabtree, M.S. Dresselhaus, MRS Bull. 33 (2008) 421–428.
[5] M.S. Dresselhaus, I.L. Thomas, Nature 414 (2001) 332–337.
[6] W. Grochala, P.P. Edwards, Chem. Rev. 104 (2004) 1283–1316.
[7] J. Alper, Science 299 (2003) 1686–1687.
[8] C. Luna, C. Macchi, A. Juan, A. Somoza, Int. J. Hydrogen Energy 35 (2010) 12421–12427.
[9] R. Yu, P.K. Lam, Phys. Rev. B 37 (1988) 8730–8737.
[10] X. Shang, M. Bououdina, Z.X. Guo, J. Alloys Compd. 349 (2003) 217–223.
[11] P. Selvam, B. Viswanathan, C.S. Swamy, V. Srinivasan, Int. J. Hydrogen Energy 11 (1986) 169–192.
[12] G. Liang, J. Alloys Compd. 370 (2004) 123–128.
[13] Y. Song, Z.X. Guo, R. Yang, Phys. Rev. B 69 (2004) 942015–942051.
[14] X.B. Xiao, W.B. Zhang, W.Y. Yu, N. Wang, B.Y. Tang, Phys. Rev. B 404 (2009) 2234–2240.
[15] S. Hao, D.S. Sholl, Appl. Phys. Lett. 93 (2008) 251901–251903.
[16] M.S. Park, A. Janotti, C.G. Van de Walle, Phys. Rev. B 80 (2009) 1–5.
[17] H.G. Schimmel, J. Huot, L.C. Chapon, F.D. Tichelaar, F.M. Mulder, J. Am. Chem. Soc. 127 (2005) 14348–14354.
[18] P. Hautojärvi, C. Corbel, in: A. Dupasquier, A.P. Mills Jr. (Eds.), Positron Spectroscopy of Solids, IOS Press, Amsterdam, 1995, pp. 491–528.
[19] S.W.H. Eijt, R. Kind, S. Singh, H. Schut, W.J. Legerstee, R.W.A. Hendrikx, J. Appl. Phys. 105 (2009) 1–13.
[20] H. Leegwater, H. Schut, W. Egger, A. Baldi, B. Dam, S.W.H. Eijt, Appl. Phys. Lett. 96 (2010) 1–3.
[21] R. Checchetto, N. Bazzanella, A. Kale, A. Miotello, S. Mariazzi, R.S. Brusa, P. Mengucci, C. Macchi, A. Somoza, W. Egger, L. Ravelli, Enhanced kinetics of hydride-metal phase transition in magnesium by vacancy clustering, Phys. Rev. B 84 (2011) 054115.
[22] W. Kohn, L.J. Sham, Phys. Rev. 140 (1965) A1133–1138.
[23] G. Kresse, D. Joubert, Phys. Rev. B 59 (1999) 1758–1775.
[24] P.E. Blöchl, Phys. Rev. B 50 (1994) 17953–17979.
[25] J.P. Perdew, Y. Wang, Phys. Rev. B 45 (1992) 13244–13249.
[26] H.J. Monkhorst, J.D. Pack, Phys. Rev. B 13 (1976) 5188–5192.
[27] B. Deb (Ed.), The Hellmann-Feynman Theorem, in the Force Concept in Chemistry, Van Nostran-Reinhold, Toronto, 1981.
[28] E.J. Baerends, D.E. Ellis, P. Ros, Chem. Phys. 2 (1973) 41–51.
[29] G. te Velde, E.J. Baerends, J. Comp. Phys. 99 (1992) 84–98.
[30] C. Fonseca Guerra, O. Visser, J.G. Snijders, G. te Velde, E.J. Baerends, 1995 METE CC-95 305.
[31] ADF 2.2.1, Theoretical Chemistry, Vrije Universiteit, Amsterdam, 1997.
[32] P. Hohenberg, W. Kohn, Phys. Rev. B 136 (1964) 864.
[33] R. Hoffmann, Solids and Surfaces: A Chemist's View of Bonding in Extended Structures, VCH, New York, 1988.
[34] M. Alatalo, B. Barbielini, M. Hakala, H. Kauppinen, T. Korhonen, M.J. Puska, K. Saarinen, P. Hautojärvi, R.M. Nieminen, Phys. Rev. B 54 (1996) 2397–2409.
[35] P. Asoka-Kumar, M. Alatalo, V.J. Ghosh, A.C. Kruseman, B. Nielsen, K.G. Lynn, Phys. Rev. Lett. 77 (1996) 2097–2100.
[36] I. Makkonen, M. Hakala, M.J. Puska, Modeling the momentum distributions of annihilating positron–electron pairs in solids, Phys. Rev. B 73 (2006) 035103:1–035103:12.
[37] E. Boroński, R.M. Nieminen, Phys. Rev. B 34 (1996) 3820–3831.
[38] M. Bortza, B. Berthevillea, G. Böttgerb, K. Yvona, J. Alloys Compd. 287 (1999) L4–6.
[39] Y. Yanpeng, F. Huaxiang, Phys. Rev. B 84 (2011) 064112.
[40] K. Laasonen, R. Nieminen, M.J. Puska, First principles study of fully relaxed vacancies in GaAs, Phys. Rev. B 45 (1992) 4122–4130.
[41] M. Saito, A. Oshiyama, Phys. Rev. B 5 (3) (1996) 7810.
[42] P. Vajeeston, P. Ravindran, H. Fjellvag, Theoretical investigations on low energy surfaces and nanowires of MgH_2, Nanotechnology 19 (2008) 275704:1–275704:6.
[43] F. Matar, Prog. Solid State Chem. 38 (2010) 1–37.
[44] A. Somoza, M.P. Petkov, K.G. Lynn, A. Dupasquier, Phys. Rev. B 65 (2002) 094107.
[45] P. Folegati, I. Makkonen, R. Ferragut, M.J. Puska, Analysis of positron–electron momentum spectra of metallic alloys as supported by first-principles calculations, Phys. Rev. B 75 (2007) 054201:1–054201:10.
[46] R.S. Brusa, W. Deng, G.P. Karwasz, A. Zecca, Nucl. Instrum. Methods B 194 (2002) 519–531.
[47] J. Čižek, I. Prochazka, S. Danis, G. Brauer, W. Anwand, R. Gemma, E. Nikitin, R. Kirchheim, A. Pundt, R.K. Islamgaliev, Hydrogen–vacancy complexes in electron-irradiated niobium, Phys. Rev. B 79 (2009) 054108:1–054108:18.
[48] A. Calloni, A. Dupasquier, R. Ferragut, P. Folegati, M.M. Iglesias, I. Makkonen, M.J. Puska, Positron localization effects on the Doppler broadening of the annihilation line: aluminum as a case study, Phys. Rev. B 72 (2005) 054112:1–054112:6.